Materials and Structures (2023) 56:112
https://doi.org/10.1617/s11527-023-02201-0

ORIGINAL ARTICLE

The structural response of masonry walls strengthened using prestressed near surface mounted GFRP bars under cyclic loading

Hossein Kanani kashani · Milad Shakiba · Milad Bazli · Seyed Mohammad Hosseini · Seyed Mohammad Reza Mortazavi · Mehrdad Arashpour

Received: 30 November 2022 / Accepted: 23 June 2023 / Published online: 11 July 2023

Abstract The preliminary findings of cyclic tests conducted on a series of half-scale unstrengthened and strengthened masonry walls are presented. Reinforced walls were strengthened by (i) non-prestressed near surface mounted (NSM) glass fibre reinforced polymer (GFRP) bars and (ii) prestressed NSM GFRP. Walls were strengthened symmetrically by vertical bars passing through both mortar and bricks. The structure was subjected to concurrent sustained uniformly distributed vertical loads and static cyclic horizontal loads. Each reinforcement method was evaluated for its loading capability and ductility efficiency. The experimental results showed a considerably higher ultimate load-carrying capability and ductility of strengthened walls compared to the unstrengthened wall. This was more pronounced for walls reinforced with prestressed GFRP bars. The ultimate strength of the strengthened walls compared to the un-reinforced masonry (USM) wall was 38% for the wall strengthened with the non-prestressed NSM technique and 58% for the wall strengthened with the prestressed NSM technique. The horizontal failure displacement was improved by about 64% in the non-prestressed NSM technique and 127% in the prestressed NSM technique compared to the USM wall.

Keywords Masonry · FRP · Retrofitting · Strengthening · Near-surface mounted · NSM · Prestressed NSM

H. K. kashani · M. Shakiba · S. M. Hosseini · S. M. R. Mortazavi
Department of Civil Engineering, Shahid Rajaee Teacher Training University, Tehran, Iran

M. Bazli (✉)
Faculty of Science and Technology, Charles Darwin University, Darwin, Australia
e-mail: milad.bazli@cdu.edu.au; m.bazli@uq.edu.au

M. Bazli
School of Mechanical and Mining Engineering, The University of Queensland, Brisbane, Australia

M. Arashpour
Department of Civil Engineering, Monash University, Melbourne, Australia

1 Introduction

Due to the rapid advancements in strengthening, it is critical to create innovative approaches that take advantage of the current Fiber Reinforced Polymer (FRP) composites. FRP offers significant advantages, including a high strength-to-weight ratio and exceptional resistance to corrosion [1–5]. Additionally, there is minimal loss of usable space due to the strengthening with FRP, as the application process is relatively simple and non-intrusive to traditional strengthening methods, such as steel plate bonding, external post-tensioning, or concrete jacketing [6, 7]. However, it is worth mentioning that applying FRP to

strengthen masonry structures can be particularly challenging, especially when dealing with uneven surfaces or the application on vault intrados. In addition to the benefits listed above, FRP reinforcement will prevent crack growth. By applying FRP composites, the tensile strength of the reinforced sections is significantly enhanced, thus inhibiting the propagation of cracks and minimising the risk of structural failure. This crack prevention mechanism plays a vital role in enhancing the overall performance and longevity of the strengthened structures [8].

Externally-bonded prestressed (EBP) fibre-reinforced polymer plates/bars and near-surface mounted (NSM) FRP strips/bars are two important techniques for strengthening concrete and masonry structures with FRP materials. However, there are considerable limitations to these two techniques, i.e. EBP and NSM. Although strengthening with externally bonded FRP composites significantly improves the flexural behaviour of strengthened beams [9], numerous research detected their premature debonding failure, limiting their ability to use the FRP composites' high-strength properties [10, 11]. Because this technique lacks strain compatibility between concrete/masonry sections and FRP, it presents numerous challenges in terms of analysis and design [12]. Additionally, environmental exposure increases the potential damage to FRP bars during the construction stage and their service life [13, 14]. Indeed FRP composites have displayed varying levels of degradation in their mechanical properties when subjected to environmental conditions such as hygrothermal, alkaline, acidic, and UV radiation exposures [15–17]. The NSM method demonstrated remarkable results in increasing beams' ultimate flexural capacity, but no substantial improvement in the pre-cracking stage was observed [18–20]. The lack of substantial improvement in the pre-cracking stage with the NSM method could be attributed to several factors. The NSM method primarily focuses on enhancing the load-carrying capacity of the members by providing additional reinforcement within the structure. While this method effectively increases the overall strength of the beams, it may not significantly improve the structure behaviour in terms of cracking initiation and propagation. Furthermore, the NSM method may not provide sufficient reinforcement in the critical regions of the members where cracking is most likely to occur. The distribution and arrangement of the NSM reinforcement might not effectively control the tensile stresses in the pre-cracking stage, leading to limited improvement in crack resistance. Also, the behaviour of the members in the pre-cracking stage is influenced by various factors such as the concrete/masonry's tensile strength, the geometry of the members, and the applied loading conditions. These factors can interact in complex ways, and the NSM method alone may not be able to completely overcome the limitations imposed by these factors.

Using prestressed NSM FRP strips/bars can combine the advantages of these two strengthening methods, and it thus becomes very attractive to promote further FRP applications in strengthening concrete and masonry structures [21]. This newly designed strengthening approach was introduced to maximise the techniques' effectiveness. This technique is presently being investigated to incorporate into design guidelines as an alternative to conventional strengthening methods [22].

Hong and Park [23] used a prestressed NSM strengthening method utilising carbon fibre-reinforced polymer (CFRP) laminates. Their research focused mostly on the influence of the initial prestressing level. The cracking, yielding, and ultimate loads of the strengthened beams were improved as a result of the strengthening. Recently, Sokairge et al. [22] investigated the efficacy of using basalt fibre-reinforced polymer (BFRP) bars for strengthening reinforced concrete (RC) beams using non-prestressed NSM and prestressed NSM techniques. Based on the results conducted on beams with varying initial prestressing levels and placements of NSM bars, it was determined that strengthening RC beams with the prestressed NSM technique provides a superior enhancement in the pre-cracking stage compared to the non-prestressed NSM technique, while reducing a significant portion of the beam's ductility.

Unstrengthened masonry (USM) structures can fail due to a lack of wall strength under lateral in-plane or out-of-plane loading, insufficient diaphragm stiffness, or weak wall-diaphragm connections [24–26]. USM structures are extremely sensitive to damage from earthquake loading due to their large seismic mass, poor tensile strength, and low ductility. FRP strengthening is gaining attraction as a cost-effective seismic strengthening option for USM walls [27]. Similar to RC structures, several techniques, such as externally bonded reinforcement (EBR) and NSM, have been

implemented to strengthen masonry structures with FRP plates/sheets and bars. For example, Jafari et al. [28] investigated the in-plane behaviour of USM walls using CFRP and glass FRP (GFRP) sheet arrays and NSM GFRP bars. They found that all strengthening methods greatly increased the loading capability and ductility of wallettes. Li et al. [29] conducted diagonal tests on large-scale wallettes constructed with block units and strengthened with near-surface mounted GFRP bars and found a 28–123% increase in strength compared to control specimens. They observed both diagonal shear and sliding shear cracks. Turco et al. [30] conducted a similar experiment with different details and observed a 70–123% strength increment. Santa-Maria et al. [31] conducted diagonal tests on 1100 × 1060 mm brick wallettes strengthened with CFRP sheets and observed an incremental strength gain of up to 70%. Hamid et al. [32] also conducted diagonal compression tests on wallettes constructed with blocks in a grid array and strengthened with GFRP sheets. They reported the highest strength, with a 358% increase in strength. Due to the simplicity, most studies have focused on monotonic static testing of FRP-strengthened masonry structures [33–35]. However, few studies investigated the performance of such structures under static cyclic and dynamic loadings. For example, Konthesingha et al. [36] evaluated the bond strength of NSM FRP strips to modern clay brick masonry prisms during cyclic loading. They found that the bond strength is approximately 20% lower under cyclic loading than under monotonic loading. The static cyclic in-plane shear response of damaged masonry walls strengthened with NSM CFRP strips was examined by Konthesingha et al. [37]. They reported that strengthening at greater pre-compression levels did not increase ultimate loads. On the other hand, the reinforcement restored the ultimate loads to those recorded in the undamaged USM state. ElGawady et al. [38] examined the efficacy of EBR GFRP and Aramid FRP (AFRP) in strengthening damaged masonry wall panels subjected to cyclic loads.

Prestressing can help address issues such as cracking, deformation, and load capacity limitations that are commonly associated with masonry structures. It allows for the redistribution of stresses within the masonry assembly, effectively reducing tensile stresses and enhancing the load-bearing capacity. Moreover, masonry prestressing techniques can be applied to both new and existing structures, making it a versatile and valuable approach for structural rehabilitation and strengthening projects. Although the impact of masonry prestressing is extensively discussed in the literature [39–46], very few studies investigated the in-plane shear performance of USM strengthened with prestressed NSM FRP bars using a static in-plane diagonal compression test. For instance, Yu et al. [47] investigated the in-plane shear performance of USM strengthened with prestressed NSM GFRP bars placed horizontally and tested under a static diagonal compression test. It was demonstrated that reinforcing USM walls with prestressed GFRP bars are suitable for closing/repointing wide cracks in existing masonry structures. Additionally, research findings indicated that prestressed bar- strengthened walls had a greater shear capacity than unstrengthened control walls or walls reinforced with non-prestressed bars. However, to investigate the efficiency of such a method during earthquakes, cyclic testing should be considered. Moreover, placing FRP bars vertically while passing through bricks and mortar rather than only mortar seems an appropriate technique that could be studied.

However, to the author's knowledge, there is no research study investigating the efficiency of the prestressed NSM strengthening technique on unstrengthened masonry structures using cyclic loading with vertical bars. Therefore, the present study addressed such a strengthening technique and evaluated its efficiency using static cyclic loading.

2 Experimental program

2.1 Materials

It is well established that the mortar strength and masonry unit (brick) contribute significantly to the in-plane resistance of unstrengthened masonry (USM) walls. The bricks used in the study had dimensions of 200 × 100 × 50 mm. The average compressive strength and elastic modulus of the 10 tested bricks, determined in accordance with ASTM C67-00 [48], were found to be 3.7 ± 0.21 MPa and 1120 ± 63.9 MPa, respectively.

The mortar employed in the study is a composition of Portland cement, sand, and water. Five 50 mm cubes were tested to determine the mechanical

properties of mortar and if they fulfil the minimal requirements of current standards. The mortar was prepared with water-to-cement and sand-to-cement ratios of 0.5 and 0.25 by weight, respectively. This test was carried out following ASTM C109 [49]. The average strength and modulus of elasticity of the mortar were 18 ± 1.31 MPa and 3.3 ± 0.24 GPa, respectively. The mortar is categorised as medium-strength. Compression tests were also performed on ten randomly selected bricks following ASTM C67-00 [50].

The commercial 4 mm GFRP bars used in this study consisted of 70% E-glass and 30% vinyl ester resin by volume. GFRP bars had an average ultimate tensile strength of 600 ± 50 MPa, tensile elastic modulus of 55 ± 5 GPa, and ultimate tensile strain of 1.2 ± 0.1% according to the manufacturer.

HIT-RE 500 V3 injection mortar Hilti Anchorage adhesive was used to strengthen NSM GFRP bars. The adhesive's tensile, flexural, and compressive strengths were 43.5 MPa, 12.4 MPa, and 82.7 MPa, respectively, after seven days of curing, as per the manufacturer's datasheet.

2.2 Specimen

Three half-scale 1200 × 1200 × 200 mm walls, including one USM wall, one strengthened with non-prestressed NSM technique and one strengthened with prestressed NSM techniques, have been prepared and tested under static cyclic loading. A mortar thickness of 30 mm was applied for each layer of the wall.

2.2.1 USM wall

Masonry walls were constructed with inner mortar between bricks and sat on a 250 × 500 × 1400 mm rectangular concrete reinforced foundation. Walls were connected to the foundation by a single layer of mortar. Walls were cured for 42 days in an ambient laboratory environment before testing. Figure 1 shows the USM and foundation configurations.

2.2.2 Non-prestressed NSM strengthened wall

The second wall was strengthened with non-prestressed NSM GFRP bars. Wall was strengthened symmetrically on both sides. To prepare for the installation of the GFRP bars, the wall surfaces were cleaned and dust was removed. Then, using a disc grinder slits 10 mm wide and 10 mm deep was carved into each side of the wall. Dust was removed from these gaps using an air blower. Then, almost half of each slit was filled with HILTI adhesive (Sect. 2.1). GFRP bars with a diameter of 4 mm were positioned and slits were filled with HILTI adhesive. After 7 days of adhesive curing, the wall was tested. The steps for applying near surface mounted bars reinforcement are shown in Fig. 2.

2.2.3 Prestressed NSM strengthened wall

The third wall was strengthened with prestressed NSM GFRP bars. An initial prestressing level of 20% of the ultimate tensile strain of GFRP bars was considered in this study. The determination of prestressing level in strengthening masonry structures depends on several factors, including the specific requirements of the project, the structural condition of the masonry, and the desired level of improvement. The prestressing level is typically determined through engineering analysis and design considerations. GFRP bars were prestressed according to the following steps:

(1) *The bottom end of the GFRP bars* The bottom end of the bars was embedded inside the foundation for a 70 mm embedment length (Fig. 3a). To place GFRP bars in the concrete foundation, the following steps were taken: First, the area where the GFRP bar would be placed was cleaned from any dirt to provide a clean bonding surface for the bar. Then a groove was created in the concrete to accommodate the bar. Then the GFRP bar was carefully inserted into the prepared area, by pushing it into place, ensuring it is fully embedded in the concrete. Finally using HILTI adhesive, the surrounding space between the bar and the concrete was filled to provide further anchorage.

(2) *The top end of the GFRP bars* In this step, the top end of the GFRP bars is prepared for prestressing. A steel tube is used to house the top end of the bars. Before inserting the bars, the inner surface of the steel tube is grooved. These grooves provide additional friction and help prevent slippage between the GFRP bar and the tube. Once the tube is prepared, it is filled with HILTI adhesive (Fig. 3b). The adhesive acts as

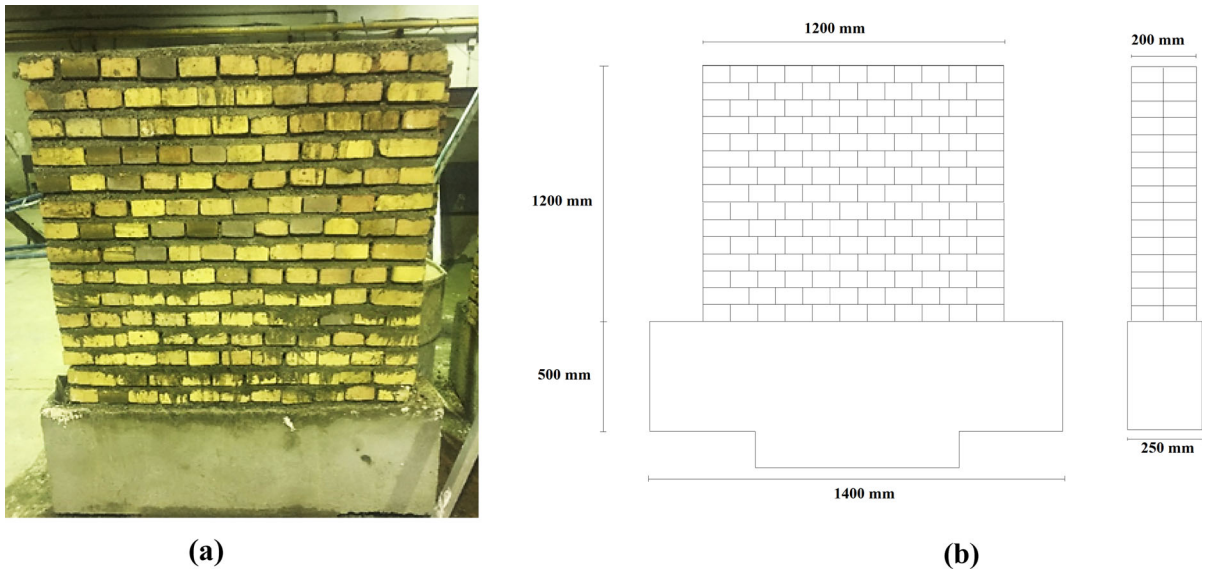

Fig. 1 USM and foundation configurations: **a** Actual wall; **b** Schematic drawing

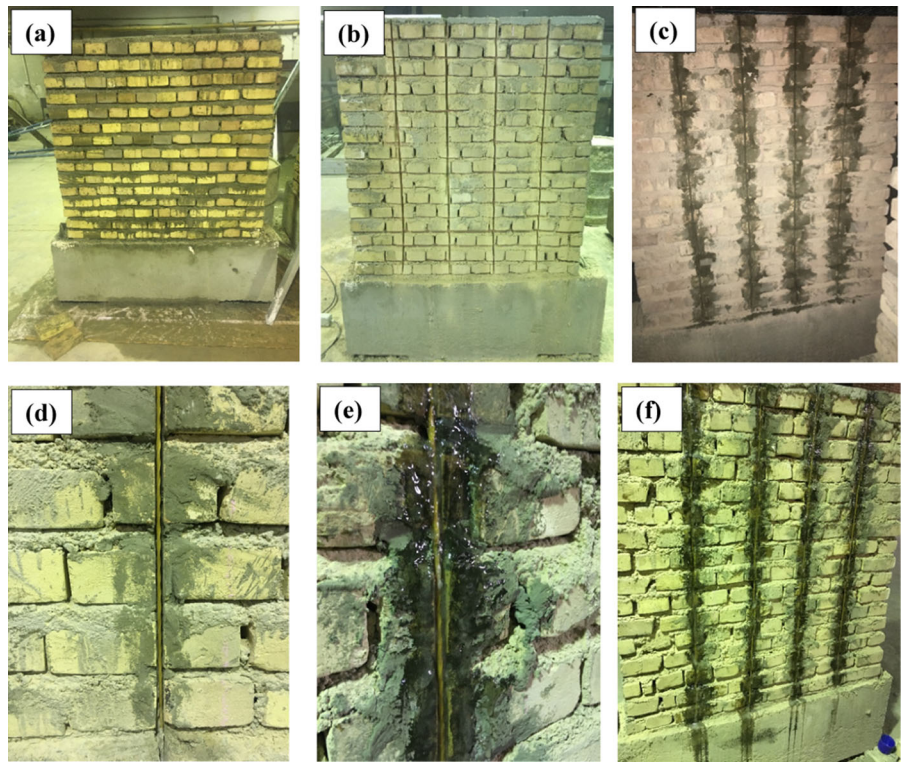

Fig. 2 Non-prestressed NSM strengthened wall: **a** USM wall; **b** Creating slits on the wall surface; **c** Filling half of the slit with mortar; **d** Placing GFRP bar inside the slit; **e** Filling the whole slit with glue; **f** final view of the non-prestressed NSM wall

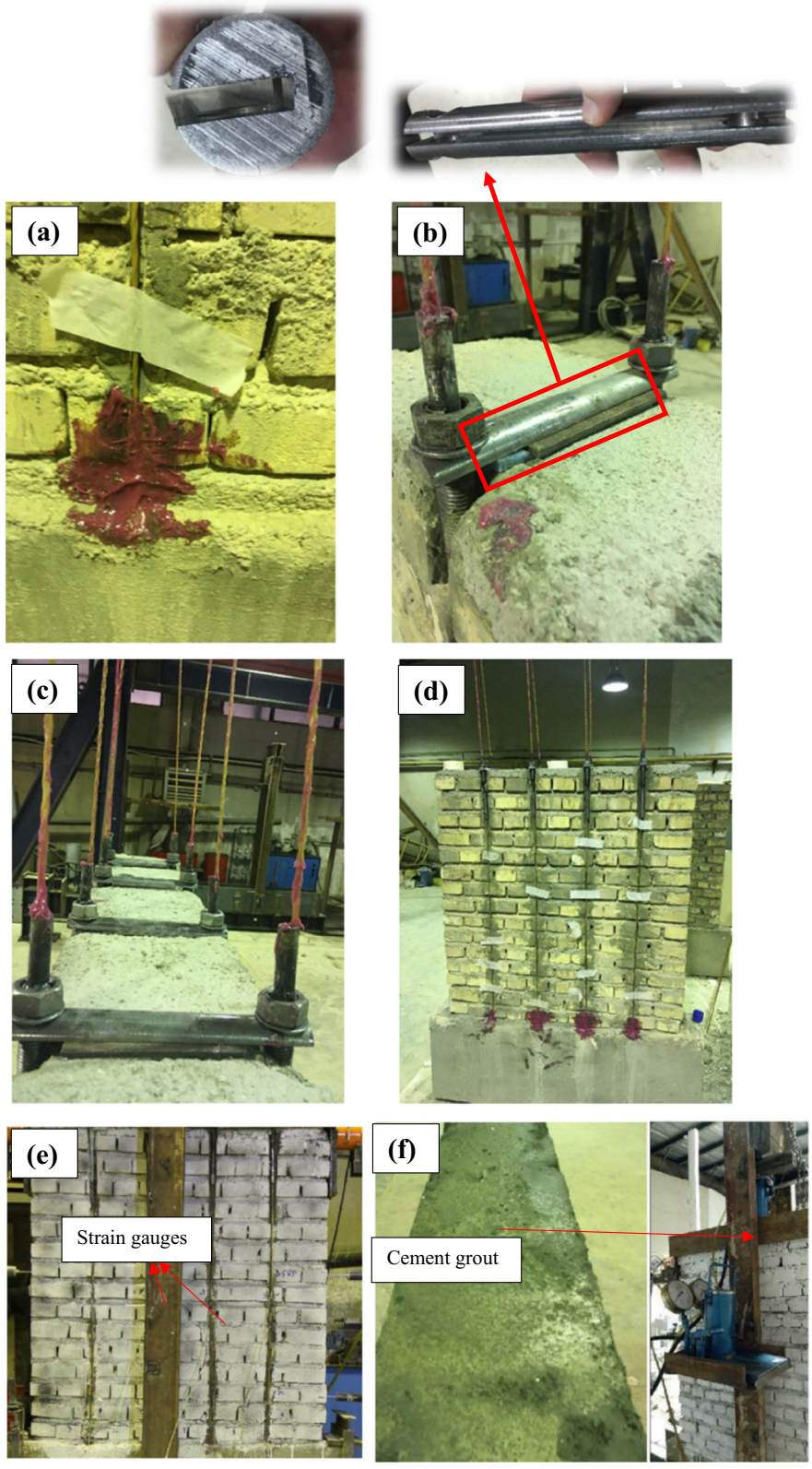

Fig. 3 Prestressed NSM strengthened wall: **a** GFRP bar embedded inside the foundation; **b** Tope end anchoring; **c** Prestressed GFRP bars; **d** final view of the prestressed NSM wall; **e** Attaching strain gauges; **f** Applying grout on the top of the wall to enable vertical loading

a bonding agent, ensuring a strong connection between the GFRP bar and the steel tube. The adhesive also helps to transfer the prestressing force from the steel tube to the GFRP bar. The top end of the GFRP bar is then carefully inserted into the steel tube, ensuring that it is fully seated and securely held in place by the adhesive. The bar should be positioned properly, and aligned with the desired direction of prestressing force.

(3) *Pulling the bars and fixing the prestressing system* After the GFRP bars are properly placed in the foundation and inside the steel tube, the bars are subjected to tension to induce prestressing. In this step, the bars are pulled to achieve a specific elongation. Steel shackles are used to connect GFRP bars on each side of the wall (Fig. 3c). The shackles are connected to the top end of the bars, which are secured inside the steel tube. The bars are gradually pulled by turning the steel anchorage nut. During the prestressing level employed in this study, no indications of masonry crushing were detected. However, it is crucial to take into account the possibility of crushing at the top portion of the wall should be considered if higher levels of prestressing load are contemplated.

A strain gauge was connected to each GFRP bar to continuously record the bar strain (Fig. 3e). The nut was tightened until the strain in the GFRP bar reached 20% of its ultimate strain. This level of strain corresponded to a vertical deformation of 3.9 mm, as measured. After installing the prestressing system on the wall, strain gauges were used to monitor the strains in the GFRP bars for any potential relaxation. However, due to the immediate testing of the prestressed wall after prestressing, the observed strain relaxation was found to be negligible. After the prestressing of the bars was completed, it is important to note that the upper section of the GFRP bars, embedded inside the steel tube, was cut (approximately 50 mm from the top surface of the wall). Subsequently, a 100 mm layer of grout was applied to the top part of the wall. This step was taken to embed the upper portion of the bar and facilitate applying of vertical load (Fig. 3f).

2.3 Test set-up

Walls were tested under sustained vertical load and static cyclic horizontal loads. A vertical load of 75 kN, equivalent to 10% of the basic ultimate axial capacity of the URM wall, F_o (Eq. 1), was applied uniformly on top of the wall through a steel I-section profile.

$$F_o = F_m{\prime}A_b \tag{1}$$

In Eq. 1, $F_m{\prime}$ is the characteristic compressive strength of the masonry and A_b is the bedded area.

A vertical hydraulic jack and load cell were placed on top of the I beam to apply and record the applied load. It is worth noting that to avoid any interaction between the wall and the I beam, the top surface of the prestressed NSM stretched beam was flattened with mortar.

Lateral static cyclic loads from both sides were applied to the top height of the beams through two steel angles. Horizontal load cells were affixed at a height of 1000 mm from the surface of the foundation. Horizontal hydraulic jacks and load cells were attached to angles to apply and record the loads. A 2 mm displacement was added to the previous step in each lateral static cycle until the wall collapsed. The displacement-controlled loading regime was applied at a 1 mm/min rate. Figure 4 shows the horizontal cyclic loading protocol used in this study.

It should be noted that the vertical jack was designed to move along its axis to avoid any misalignment of the vertical load due to the horizontal movement of the walls. Two I-beams laterally supported all beams at their mid-length to avoid any out-of-plan movement. In addition, the foundation was fixed to the ground by welding it to a steel frame to avoid lateral movement and uplifting.

Figure 5 shows the test set-up and the location of the LVDTs, hydraulic jacks, and load cells used in this

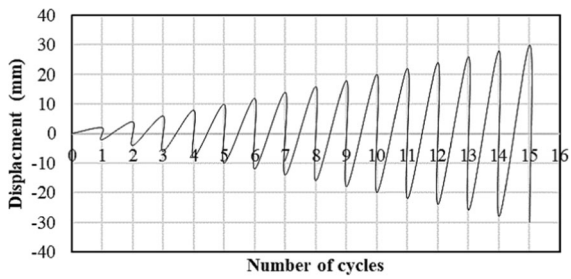

Fig. 4 Horizontal cyclic loading protocol

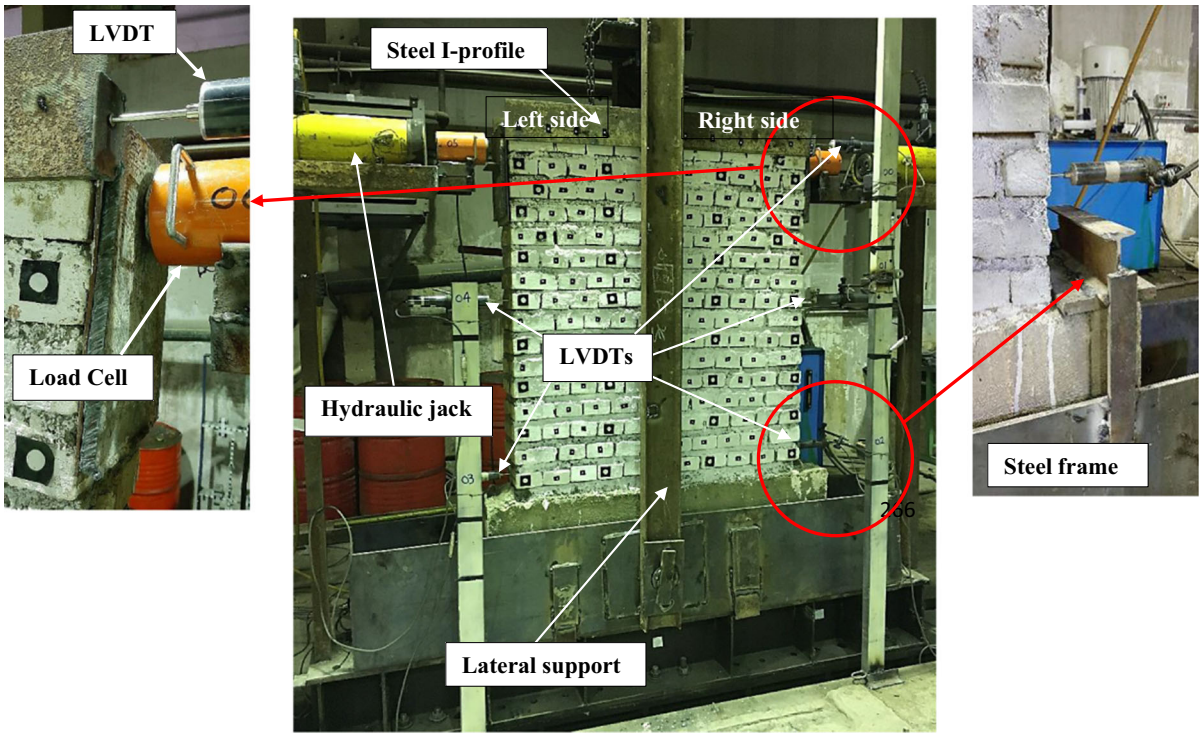

Fig. 5 Test set-up

study. Five linear variable differential transformers (LVDTs) were attached horizontally to the walls to measure the wall's horizontal displacements during the tests continuously. Specifically, two LVDTs were positioned at the mid-height of the wall, precisely 600 mm from the surface of the foundation. Additionally, another two LVDTs were placed at a level 150 mm above the foundation surface. The fifth LVDT was attached at the topmost section of the wall, precisely 1200 mm from the foundation surface. An automatic data logger was used to record the data produced by LVDTs and load cells.

3 Results and discussion

Table 1 summarises the experimental results of tested walls in terms of the maximum horizontal loads ($F_{h,\max}$) and the maximum horizontal displacements ($d_{\max}$) for left and right directions, initial stiffness (K_i) and failure modes. The initial stiffness of specimens was determined by dividing the maximum load experienced during the first cycle by the corresponding maximum displacement observed within the first cycle. There are two significant differences between the prestressed and non-prestressed strengthened specimens that contribute to their distinct stiffness behaviours. Firstly, in the non-prestressed wall, the GFRP bars were embedded in adhesive, establishing direct contact with the bricks. In contrast, the GFRP bars in the prestressed wall were anchored at the top and bottom without being covered in adhesive. This disparity in bonding conditions influences the load transfer mechanism between the GFRP bars and the surrounding materials, resulting in variations in stiffness. Secondly, the GFRP bars in the prestressed wall were embedded in the concrete foundation, effectively transferring the load to the foundation. Conversely, this load transfer mechanism was absent in the non-prestressed wall. The presence or absence of load transfer to the foundation impacts the overall stiffness response of the walls.

The following sections discuss walls failure mode, load-deflection curves and stiffness variations in detail.

Table 1 Experimental results of tested walls

Wall Type	$F_{h,\ max}$ (kN)	$d_{max\ left}$	$d_{max,\ right}$	K_i (kg/m)	Failure mode
USM	38.3	20	20	1015	Diagonal shear crack
Non-prestressed NSM	53	42	40	6000	Toe crushing
Prestressed NSM	60.6	56	46	3049	Bond failure (sliding) + diagonal shear crack + bar pull-out

3.1 Failure modes

The in-plane failure modes of masonry walls can be classified into four primary categories (Fig. 6) [38, 51]. These failure mechanisms can occur during earthquakes and, depending on their severity along the masonry wall, have the potential to cause complete wall collapse [24]. These failure types begin with the formation of narrow cracks. With increasing loading or movement, the entire wall may collapse, or a portion of the wall may fail.

3.1.1 USM wall

Wall 1 (i.e. USM wall) failed due to the diagonal shear crack, which led to the destruction and collapse of the wall (Fig. 6a). Diagonal cracks may run through bricks, mortar joints, or a combination of both, depending on the strength of each component. In the case of USM, the crack has propagated through the mortar joists. The first crack started at the bottom corner of the wall in the second cycle (drift of 4 mm and maximum load of 3kN) (i.e. the first row of the

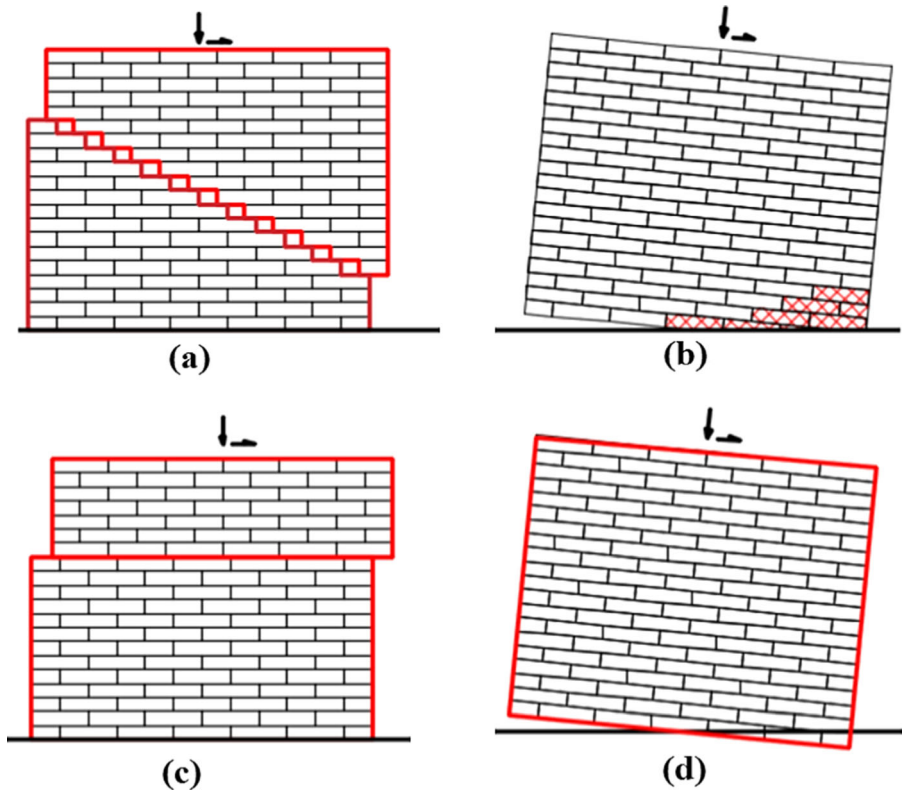

Fig. 6 Typical in-plane failure modes of masonry walls: **a** diagonal shear failure; **b** Toe crushing; **c** Sliding (bond failure); (d) Rocking

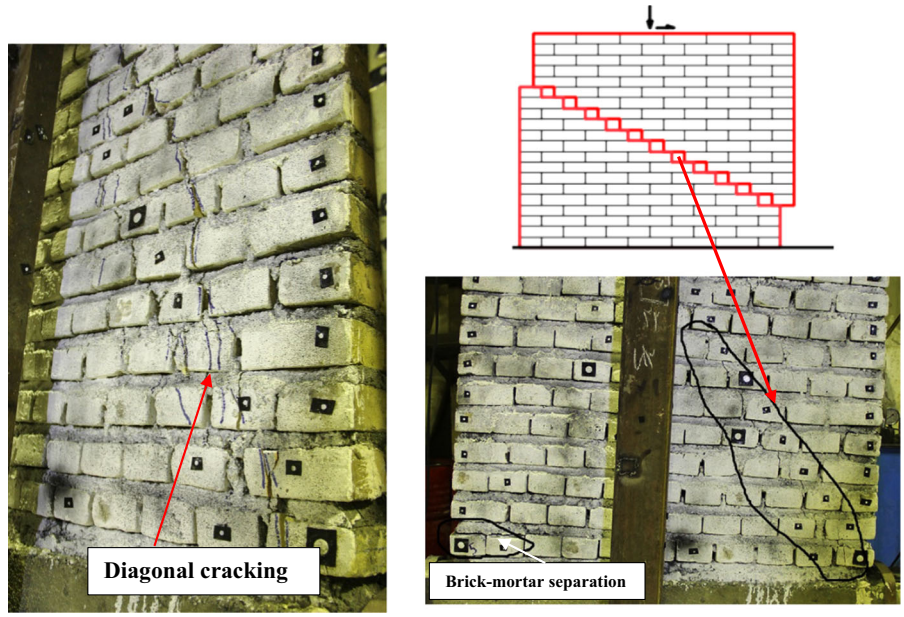

Fig. 7 Failure mode observed in USM wall

bricks on top of the foundation). It propagated upward diagonally until the total collapse at the maximum horizontal displacement of 20 mm. Figure 7 shows the failure mode observed in the USM wall. It is important to clarify that the marked line serves solely to indicate the specific area that experienced cracking or failure and it does not represent a crack or failure mode itself.

3.1.2 Non-prestressed NSM strengthened wall

Non-prestressed NSM strengthened wall has failed due to the crushing (Fig. 6b). Tension cracks form at the wall's tension bed joints as horizontal force or lateral displacement of the top of the wall grows, whereas the compression part carries both compression and shear loads. In the case of walls strengthened with non-prestressed NSM GFRP bars, the applied loads are transferred through the bars to the bottom row of the wall. As a result, during the initial cycle (drift of 2 mm drift and maximum load of 12 kN), the first brick at the bottom corner starts to detach from the mortar. In the fifth cycle (drift of 10 mm and maximum load of 18 kN), initial cracks at the wall corner appear. Eventually, at the eighteenth cycle (drift of 36 mm and maximum load of 49 kN), due to the high stiffness of the foundation (i.e. no rocking failure), crushing of the corner (toe crushing) happened in a non-prestressed NSM strengthened wall. The test was continued for three more cycles (drift of 42 mm and maximum load of 53 kN) until diagonal cracking occurred and the wall completely collapsed. However, 36 mm was considered the failure deflection of this wall since the wall has lost its functionality at this cycle. Figure 8 shows the failure mode observed in the non-prestressed NSM strengthened wall. The analysis of Fig. 8 reveals the occurrence of rocking at the initial stage of damage occurrence. This rocking behaviour emerges as a consequence of tension in the lower joint, leading to an opening of the joint and subsequent rotation of the wall. It is crucial to note that this initial rocking effect can have significant implications on the damage sustained by the wall with NSM strengthening. The observed rocking phenomenon can trigger a chain reaction of structural responses, potentially culminating in toe crushing and eventual failure of the wall. As the tension-induced rocking persists, the forces exerted on the wall's lower joint become intensified, imposing high compressive loads on the toe region of the wall. The concentrated stresses in this area can eventually lead to localised crushing, compromising the integrity of the wall.

3.1.3 Prestressed NSM strengthened wall

Due to the strengthening technique, this wall transfers the highest load to the foundation among all three

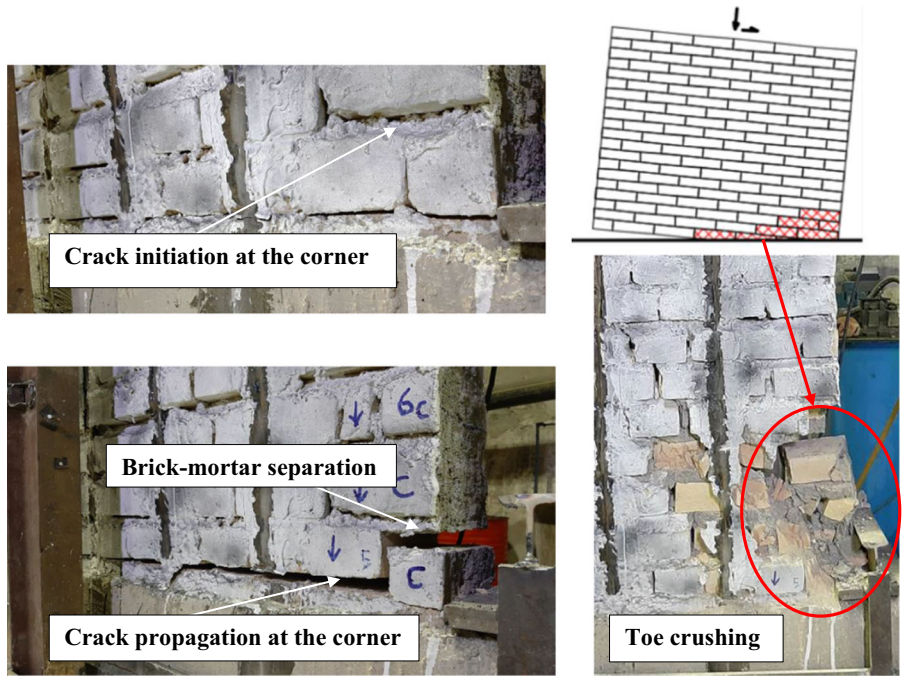

Fig. 8 Failure mode observed in non-prestressed NSM strengthened wall

types. During the third cycle (drift of 6 mm and maximum load of 15 kN), cracks started at both the left and right bottom corners (Fig. 9a). However, since GFRP bars are embedded in the concrete foundation, sliding has occurred at higher-level rows rather than bottom rows. During the seventh cycle (drift of 14 mm and maximum load of 22 kN), the sliding occurred at the third row from the bottom (Fig. 9b). This failure was observed during the sixth cycle. This failure mode can occur when the bond strength between mortar joints and bricks controls the wall capacity. This occurred because the wall's ultimate strength was significantly enhanced due to the presence of pre-stressed NSM bars, which failed to shift from diagonal mortar cracking in USM and toe crushing in non-prestressed NSM walls to bond failure (sliding) in prestressed NSM strengthened walls. Diagonal shear cracks were initiated after sliding failure at the end of the eighth cycle (drift of 16 mm and maximum load of 24 kN) (Fig. 9c). At the ninth cycle (drift of 18 mm and maximum load of 26 kN), after foundation cracking (Fig. 9d), one of the GFRP bars experienced out-of-plane buckling and became dislodged from the prestressing casing (Fig. 9e). However, all other bars were still in place and transferring the applied loads. At the end of the thirteenth cycle (drift of 26 mm and maximum load of 30 kN), a GFRP bar is pull-out together with concrete from the foundation (Fig. 9f). From the subsequent cycles until the twentieth cycle (drift of 40 mm and maximum load of 45 kN), pulling-out failure was observed in all GFRP bars. Immediately after the last GFRP bar was pulled out from the foundation, diagonal cracks were propagated, and the wall collapsed at cycle 22 (drift of 44 mm and maximum load of 60 kN). Figure 9g shows the combined failure modes observed in the masonry wall.

3.2 Load–displacement behaviour

This section will describe the behaviour of strengthened walls compared to the unstrengthened wall. Figure 10 shows the USM and strengthened walls' last cycle displacement versus load curves. As is seen, the ultimate loads of the strengthened walls were significantly improved compared to the USM (by 38% in the non-prestressed NSM technique and 58% in the prestressed NSM technique). The displacement capacity improved by about 64% in the non-prestressed NSM technique and 127% in the prestressed NSM technique compared to the USM wall. Figure 11 compares the hysteresis curves of the three tested walls. Comparing the hysteresis curves of

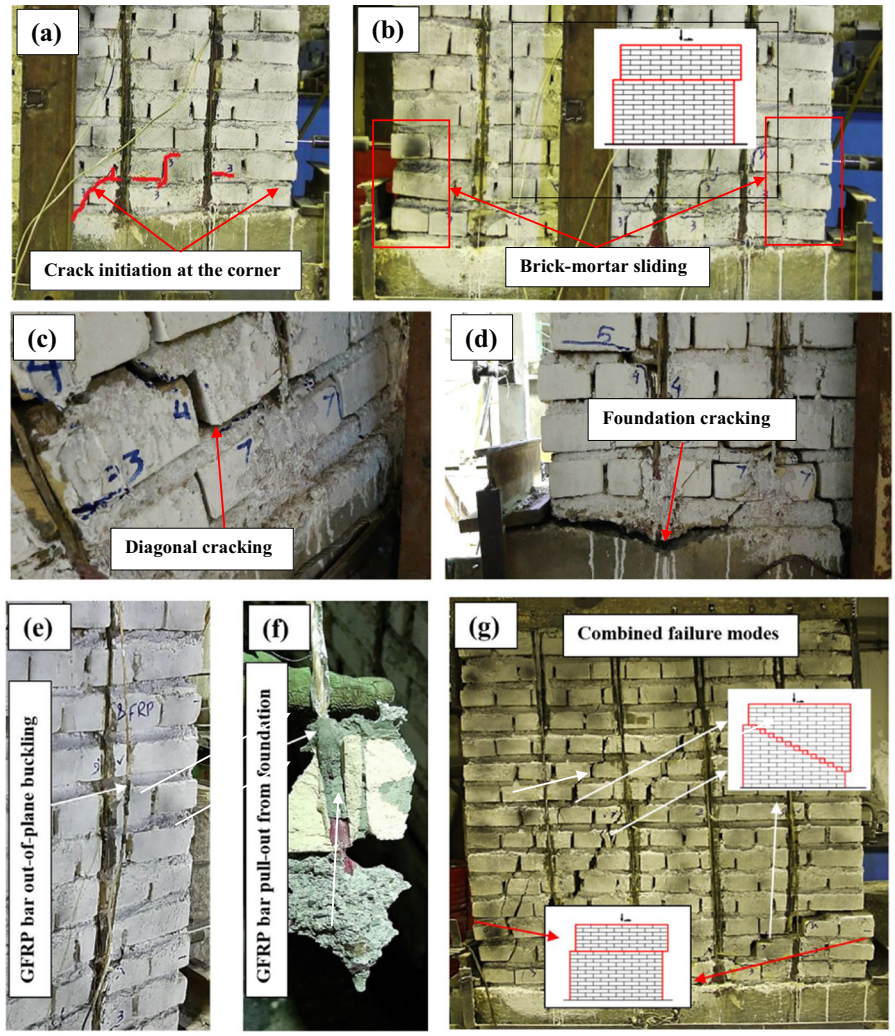

Fig. 9 Failure modes observed in prestressed NSM strengthened wall: **a** Crack initiation; **b** Brick-mortar initiation; **c** diagonal shear cracking; **d** foundation cracking; **e** GFRP bar bucking; **f** GFRP bar pull-out; **g** Different failure modes observed

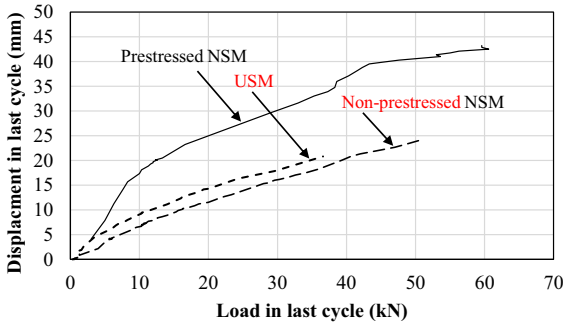

Fig. 10 Last cycle displacement-load curves of tested walls

strengthened samples, one could observe that the wall strengthened with prestressed NSM shows more ductility than that of the wall reinforced with the non-prestressed NSM technique. It can also be seen that the dissipated energy (i.e. the cumulative area under the load–displacement curves) of the wall strengthened with prestressed NSM GFRP bars is the highest. The wall reinforced with non-prestressed NSM GFRP bars showed lower energy dissipation than the prestressed NSM method. However still much higher than that of the USM wall.

Figure 12 shows the maximum load at each cycle versus the maximum displacement at the corresponding cycles of strengthened walls. As is seen in the wall strengthened with non-prestressed NSM bars, due to the mortar fractures and crack initiations, the wall shows a drop in the maximum load at several cycles compared to the previous cycle. However, the presence of the GFRP bars prevents progressive failure

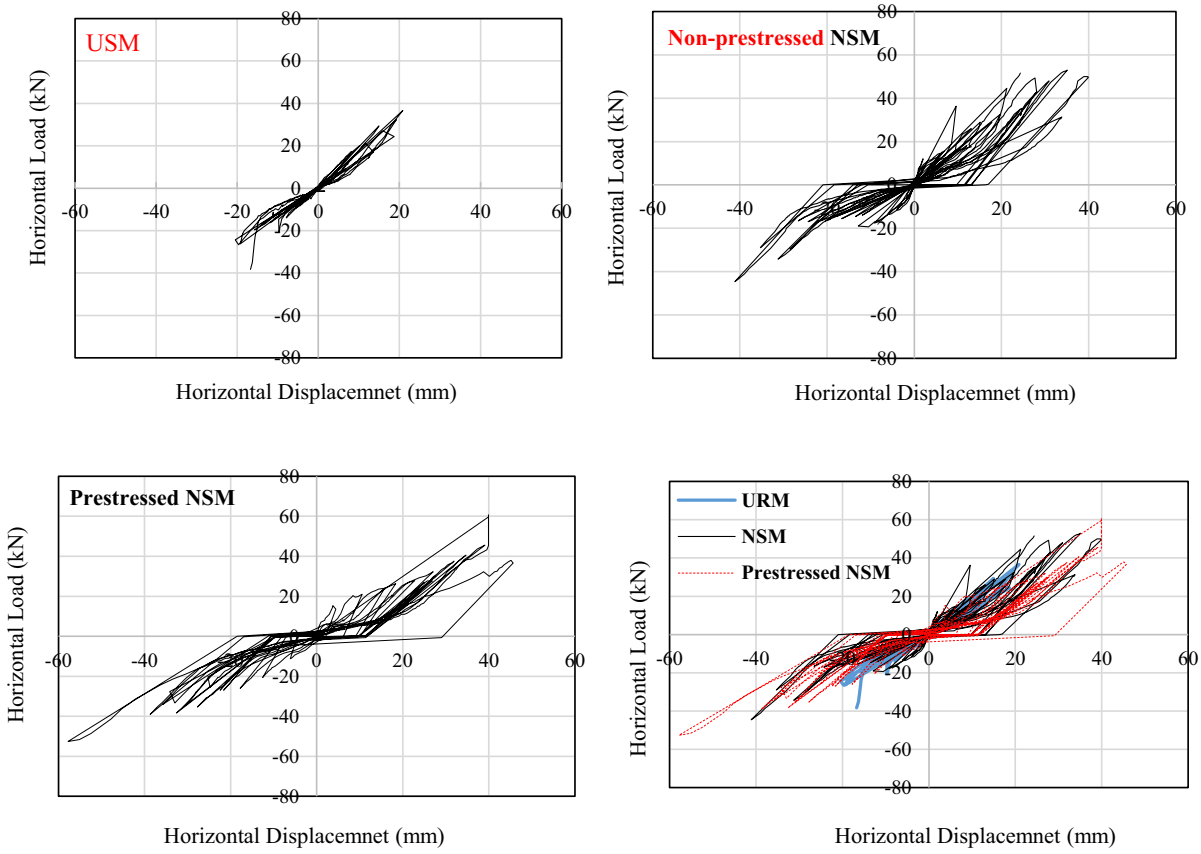

Fig. 11 Hysteresis curves of the tested walls

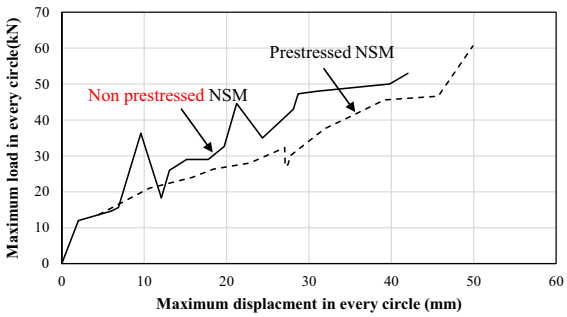

Fig. 12 Maximum load versus displacement at the end of each cycle

and crack propagation leading to a further increase in the applied load during the test.

Since most of the applied loads are directly resisted and transferred to the foundation by the GFRP bars, such a phenomenon was not generally observed in the wall strengthened with prestressed NSM GFRP, and the maximum applied load at each cycle is continuously increasing by increasing the number of cycles. This behaviour is similar to reinforced concrete structures. It is worth mentioning that a small drop in the curve of the prestressed NSM reinforced wall is due to the shear crack at the foundation.

The ultimate load and the corresponding horizontal displacement, at which the initial significant failure occurs in the wall, are compared to assess the effectiveness of two distinct strengthening methods. The wall strengthened with prestressed NSM GFRP bars resisted almost 60 kN at 44 mm drift without showing a major cracking, while the wall strengthened with non-prestressed NSM GFRP resisted 50 kN at 41 mm drift before the major failure (i.e. toe crushing). Therefore, one could conclude that in terms of both ductility and load-carrying capacity, prestressing FRP reinforcing bars are beneficial and improve the strengthening capacity of the non-prestressed NSM strengthening method for masonry walls. However, it

should be noted that the effect of the prestressing level of the FRP bar should be taken into account since it can be limited by the (residual) load-bearing capacity of strengthened masonry walls. Generally, the prestressing level is determined based on a balance between the desired structural improvement, the available resources, and the technical feasibility of implementing the prestressing method. It is typically carried out by qualified structural engineers or designers with expertise in masonry strengthening techniques.

3.3 Stiffness

The stiffness of each specimen related to each cycle was determined by dividing the maximum load experienced during each cycle by the corresponding maximum displacement observed within that cycle. Figure 13 shows the stiffness changes of strengthened samples with respect to the drift ratio. As mentioned earlier, the non-prestressed wall exhibits a higher level of stiffness in comparison to the prestressed wall, primarily attributed to the presence of resin and reinforcement bars in direct contact with the brick. Remarkably, throughout the entire duration of the test, the non-prestressed wall consistently demonstrates a higher stiffness value when compared to the prestressed wall. As is seen in Fig. 13, during some cycles, the stiffness of the non-prestressed NSM wall increases by increasing the drift ratio. This is because, after each mortar fracture or mortar-brick detachment (stiffness reduction), GFRP bars start to interact with the system and resist the wall movement and crack propagation (stiffness increment). These up-and-down steps continue until the total collapse of the wall. In contrast, the third specimen behaves differently due to the specific arrangement of the reinforcement bars. The reinforcement bars in the third specimen effectively transfer their force to the footing from the initial stages of loading. As a result, there are no significant fluctuations or notable changes in hardness observed in the third specimen throughout the test. This behaviour can be attributed to the immediate engagement of the reinforcement bars in load transfer, providing a more consistent and predictable response in terms of stiffness variations.

To understand the permanent deformation of the wall after each cycle, Fig. 14 depicts the wall's residual displacement versus drift ratio reinforced with prestressed GFRP bars. Residual displacement is calculated by the difference between the applied deformation and the recorded value from the LVDT at the end of each cycle. As expected, the residual displacement has the lowest value (about 8 mm) in the first cycle and the highest value (about 30 mm) in the last cycle. Between those cycles, the residual displacement remained constant (about 10 mm), which confirms the efficiency of the strengthening method used. In other words, the absence of a significant increase in residual displacement with increasing cycles signifies that there is no substantial damage or significant nonlinear behaviour occurring until the last cycle. Therefore, the constant residual displacement throughout the cycles serves as evidence of the method's efficiency in preventing excessive residual displacement in the masonry structure.

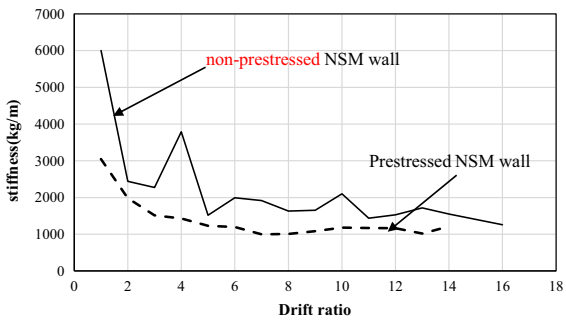

Fig. 13 Stiffness variation versus drift ratio of strengthened walls

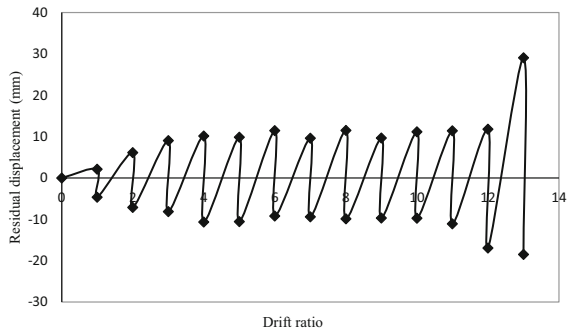

Fig. 14 Residual displacement versus drift ratio of prestressed NSM wall

4 Limitations and recommendations for future studies

In this study, there is a limitation regarding the number of experimental specimens utilised, with only one specimen of each type being tested. This limited sample size prevents a comprehensive statistical evaluation of the obtained results, and therefore, the results and conclusions should be considered indicative rather than definitive.

To overcome this limitation and enhance the reliability of the findings, conducting further experimental and numerical studies with an increased number of specimens is recommended. By expanding the sample size, a more robust dataset can be obtained, allowing for more rigorous statistical analysis and validation of the results. This will provide a solid foundation for drawing concrete conclusions and making more reliable inferences.

Furthermore, future studies should focus on exploring additional variables and parameters to gain a deeper understanding of the subject matter. By investigating a wider range of conditions, such as different loading scenarios or variations in material properties, the generalisability of the results can be improved. Moreover, incorporating more advanced numerical modelling techniques, such as finite element analysis, can complement the experimental investigations and provide a comprehensive understanding of the behaviour under consideration.

Another recommendation for future study could be to consider embedding the prestressed bars into adhesive-filled grooves. While the current study did not fill the grooves with adhesive, this alternative approach could potentially enhance the prestressing effect and alter the failure mode of the wall. Embedding prestressed bars into adhesive-filled grooves would provide a more uniform distribution of prestressing forces along the height of the wall. This could lead to improved load transfer and potentially change the failure behaviour of the strengthened wall.

The long-term relaxation behaviour of prestressed bars can impact the performance of the strengthened structure. For future studies, it is recommended to consider monitoring the relaxation of the prestressed bars over time and taking its effects into account when evaluating the effectiveness of the proposed strengthening method.

In order to advance the understanding and optimisation of prestressed NSM strengthening in masonry structures, it is recommended that future studies explore the effects of different prestressing levels. The investigation of various prestressing levels can provide valuable insights into the behaviour of the strengthened masonry walls. The outcomes of such studies will provide essential guidance for engineers and practitioners in selecting the appropriate prestressing forces to achieve optimal performance and reliability in prestressed NSM strengthening of masonry structures.

5 Conclusion

Static cyclic tests were carried out on three half-scale masonry walls, including one USM wall, one strengthened wall with non-prestressed NSM GFRP bars, and one with prestressed NSM GFRP bars. Based on the experimental test results, the following are some conclusions:

- USM walls' ultimate load caring capacity increased by 38% for the wall strengthened with the non-prestressed NSM technique and 58% for the wall strengthened with the prestressed NSM technique. The observed results confirm the efficiency of prestressing FRP bars for strengthening techniques.
- The horizontal failure displacement of USM walls increased by about 64% for the wall strengthened with the non-prestressed NSM technique and 127% in the prestressed NSM technique compared to the USM wall. This further confirms the significance of the proposed strengthening method.
- Non-prestressed NSM and prestressed NSM GFRP strengthening methods significantly improve the energy dissipation of USM walls. Wall strengthened with non-prestressed NSM bars and prestressed NSM bars failed after 18 and 22 cycles, respectively, while the USM specimen failed after only ten cycles.
- USM fails due to the propagation of diagonal shear crack passing through mortar, while non-prestressed NSM GFRP and prestressed NSM GFRP walls fail due to the toe crashing and sliding, followed by GFRP bars pull-out from the concrete foundation, respectively.

- Using a foundation with higher compressive strength (to avoid or delay bar pulling-out failure) would further enhance the efficiency of the prestressed NSM FRP strengthening method.

Acknowledgements The support of Dr. Asghar Vatani Oskouei in terms of providing the materials, technical advice and resources is greatly acknowledged.

Funding Open Access funding enabled and organized by CAUL and its Member Institutions. The authors did not receive support from any organization for the submitted work.

Declarations

Competing interests The authors have no relevant financial or non-financial interests to disclose.

Ethics approval This article does not contain any studies with human participants or animals performed by any of the authors.

References

1. Bazli M, Heitzmann M, Hernandez BV (2021) Hybrid fibre reinforced polymer and seawater sea sand concrete structures: a systematic review on short-term and long-term structural performance. Constr Build Mater 301:124335
2. Bazli M, Zhao X-L, Jafari A, Ashrafi H, Raman RS, Bai Y, Khezrzadeh H (2021) Durability of glass-fibre-reinforced polymer composites under seawater and sea-sand concrete coupled with harsh outdoor environments. Adv Struct Eng 24(6):1090–1109
3. Doostmohamadi A, Karamloo M, Oskouei AV, Shakiba M, Kheyroddin A (2022) Enhancement of punching strength in GFRP reinforced single footings by means of handmade GFRP shear bands. Eng Struct 262:114349
4. Bazli M, Heitzmann M, Hernandez BV (2022) Durability of fibre-reinforced polymer-wood composite members: an overview. Compos Struct 295:115827
5. Abolfazli M, Reyes RIJ, Choong D, Bazli M, Rajabipour A, Pourasiabi H, Arashpour M (2023) Bond behaviour between CFRP, GFRP, and hybrid C-GFRP tubes and seawater sea sand concrete after exposure to elevated temperatures. Constr Build Mater 392:131884
6. Amran YM, Alyousef R, Alabduljabbar H, Alaskar A, Alrshoudi F (2020) Properties and water penetration of structural concrete wrapped with CFRP. Results Eng 5:100094
7. Ge W, Tang R, Wang Y, Zhang Z, Sun C, Yao S, Lu W (2022) Flexural performance of ECC-concrete composite beams strengthened with carbon fiber sheet. Results Eng 13:100334
8. Oskouei AV, Kivi MP, Araghi H, Bazli M (2017) Experimental study of the punching behavior of GFRP reinforced lightweight concrete footing. Mater Struct 50(6):1–14
9. Godat A, Chaallal O, Obaidat Y (2020) Non-linear finite-element investigation of the parameters affecting externally-bonded FRP flexural-strengthened RC beams. Results Eng 8:100168
10. Wan B, Jiang C, Wu Y-F (2018) Effect of defects in externally bonded FRP reinforced concrete. Constr Build Mater 172:63–76
11. Correia L, Teixeira T, Michels J, Almeida JA, Sena-Cruz J (2015) Flexural behaviour of RC slabs strengthened with prestressed CFRP strips using different anchorage systems. Compos B Eng 81:158–170
12. Aparicio AC, Ramos G, Casas JR (2002) Testing of externally prestressed concrete beams. Eng Struct 24(1):73–84
13. Ahmadi H, Shakiba M, Mortazavi SMR, Bazli M, Azimi Z (2023) Feasibility of using static-cast concrete transmission poles fully reinforced with glass-fibre reinforced polymer bars and stirrups: a case study. Case Stud Constr Mater 18:e01780
14. Shakiba M, Ahmadi H, Mortazavi SMR, Bazli M, Azimi Z (2023) A case study on the feasibility of using static-cast fibre-reinforced concrete electric poles fully reinforced with glass fibre reinforced polymer bars and stirrups. Results Eng 17:100746
15. Bazli M, Benny B, Rajabipour A, Pourasiabi H, Heitzmann MT, Arashpour M (2023) Residual compressive strength of seawater sea sand concrete filled hybrid carbon-glass fibre reinforced polymer tubes under seawater: effects of fibre type and orientation. J Build Eng 70:106383
16. Shakiba M, Bazli M, Karamloo M, Doostmohamadi A (2023) Bond between sand-coated GFRP bars and normal-strength, self-compacting, and fiber-reinforced concrete under seawater and alkaline solution. J Compos Constr 27(1):04022098
17. Bazli M, Zhao X-L, Jafari A, Ashrafi H, Bai Y, Raman RS, Khezrzadeh H (2020) Mechanical properties of pultruded GFRP profiles under seawater sea sand concrete environment coupled with UV radiation and moisture. Constr Build Mater 258:120369
18. Abdallah M, Al Mahmoud F, Khelil A, Mercier J, Almassri B (2020) Assessment of the flexural behavior of continuous RC beams strengthened with NSM-FRP bars, experimental and analytical study. Compos Struct 242:112127
19. Sharaky I, Baena M, Barris C, Sallam H, Torres L (2018) Effect of axial stiffness of NSM FRP reinforcement and concrete cover confinement on flexural behaviour of strengthened RC beams: experimental and numerical study. Eng Struct 173:987–1001

20. Hassan T, Rizkalla S (2003) Investigation of bond in concrete structures strengthened with near surface mounted carbon fiber reinforced polymer strips. J Compos Constr 7(3):248–257
21. Peng H, Zhang J, Cai C, Liu Y (2014) An experimental study on reinforced concrete beams strengthened with prestressed near surface mounted CFRP strips. Eng Struct 79:222–233
22. Sokairge H, Elgabbas F, Elshafie H (2022) Structural behavior of RC beams strengthened with prestressed near surface mounted technique using basalt FRP bars. Eng Struct 250:113489
23. Hong S, Park S-K (2016) Effect of prestress and transverse grooves on reinforced concrete beams prestressed with near-surface-mounted carbon fiber-reinforced polymer plates. Compos B Eng 91:640–650
24. Bruneau M (1994) State-of-the-art report on seismic performance of unreinforced masonry buildings. J Struct Eng 120(1):230–251
25. Mahmood H, Ingham JM (2011) Diagonal compression testing of FRP-retrofitted unreinforced clay brick masonry wallettes. J Compos Constr 15(5):810–820
26. Giaretton M, Dizhur D, da Porto F, Ingham J (2015) Constituent material properties of New Zealand unreinforced stone masonry buildings. J Build Eng 4:75–85
27. Oskouei AV, Jafari A, Bazli M, Ghahri R (2018) Effect of different retrofitting techniques on in-plane behavior of masonry wallettes. Constr Build Mater 169:578–590
28. Jafari A, Oskouei AV, Bazli M, Ghahri R (2018) Effect of the FRP sheet's arrays and NSM FRP bars on in-plane behavior of URM walls. J Build Eng 20:679–695
29. Li T, Galati N, Tumialan JG, Nanni A (2005) Analysis of unreinforced masonry concrete walls strengthened with glass fiber-reinforced polymer bars. ACI Struct J 102(4):569
30. Turco V, Secondin S, Morbin A, Valluzzi M, Modena C (2006) Flexural and shear strengthening of un-reinforced masonry with FRP bars. Compos Sci Technol 66(2):289–296
31. Santa-Maria H, Duarte G, Garib A (2004) Experimental investigation of masonry panels externally strengthened with CFRP laminates and fabric subjected to in-plane shear load. In: 8th US National Conference on Eartquake Engineering, San Francisco, USA
32. Hamid AA, El-Dakhakhni WW, Hakam ZH, Elgaaly M (2005) Behavior of composite unreinforced masonry–fiber-reinforced polymer wall assemblages under in-plane loading. J Compos Constr 9(1):73–83
33. Willis CR, Seracino R, Griffith M (2010) Out-of-plane strength of brick masonry retrofitted with horizontal NSM CFRP strips. Eng Struct 32(2):547–555
34. Petersen RB, Masia MJ, Seracino R (2010) In-plane shear behavior of masonry panels strengthened with NSM CFRP strips. I: experimental investigation. J Compos Constr 14(6):754–763
35. Petersen RB, Masia MJ, Seracino R (2010) In-plane shear behavior of masonry panels strengthened with NSM CFRP strips. II: finite-element model. J Compos Constr 14(6):764–774
36. Konthesingha K, Masia M, Petersen R, Page A (2009) Bond behaviour of NSM FRP strips to modern clay brick masonry prisms under cyclic loading. In: Proceedings of the 11th Canadian masonry symposium
37. Konthesingha K, Masia MJ, Petersen RB, Mojsilovic N, Simundic G, Page AW (2013) Static cyclic in-plane shear response of damaged masonry walls retrofitted with NSM FRP strips–an experimental evaluation. Eng Struct 50:126–136
38. ElGawady MA, Lestuzzi P, Badoux M (2007) Static cyclic response of masonry walls retrofitted with fiber-reinforced polymers. J Compos Constr 11(1):50–61
39. Preciado A, Ramírez-Gaytan A, Gutierrez N, Vargas D, Falcon JM, Ochoa G (2018) Nonlinear earthquake capacity of slender old masonry structures prestressed with steel, FRP and NiTi SMA tendons. Steel Compos Struct 26(2):213–226
40. Moon F, Yi T, Leon R, Kahn L (2002) Retrofit of unreinforced masonry structures with FRP overlays and post-tensioning. In: Rehabilitating and repairing the buildings and bridges of Americas: hemispheric Workshop on future directions, pp. 20–36.
41. Ma R, Jiang L, He M, Fang C, Liang F (2012) Experimental investigations on masonry structures using external prestressing techniques for improving seismic performance. Eng Struct 42:297–307
42. Hwang S-H, Kim S, Yang K-H (2020) In-plane seismic performance of masonry wall retrofitted with prestressed steel-bar truss. Earthq Struct 19(6):459
43. Bayraktar A, Bayraktar S, Hökelekli E (2023) Strengthening techniques for masonry domes: a review. Int J Space Struct 38(1):30–39
44. Babatunde SA (2017) Review of strengthening techniques for masonry using fiber reinforced polymers. Compos Struct 161:246–255
45. Shrive NG, Masia MJ, Lissel SL (2001) Strengthening and rehabilitation of masonry using fibre reinforced polymers. Universidad de Calgary, Deparamento de Ingeniería Civil, Calgary, Alberta, Canadá
46. Micelli F, Cascardi A, Marsano M (2016) Seismic strengthening of a theatre masonry building by using active FRP wires. In: Brick and Block Masonry: proceedings of the 16th international brick and block masonry conference, pp. 753–761. CRC Press Padova, Italy.
47. Yu P, Silva P, Nanni A (2017) In-plane performance of unreinforced concrete masonry strengthened with prestressed GFRP bars. J Compos Constr 21(1):04016064
48. C. ASTM, 67-03 (2003) Standard test methods for sampling and testing brick and structural clay tile. American Society for Testing and Materials, Philadelphia
49. ASTM C109/C109M-16a (2016) Standard test method for compressive strength of hydraulic cement mortars (Using 2-in. or [50-mm] cube specimens). ASTM International, West Conshohocken
50. ASTM C67-00 (2002) Standard test methods for sampling and testing brick and structural clay tile. ASTM International, West Conshohocken
51. ElGawady M, Lestuzzi P, Badoux M (2006) Retrofitting of masonry walls using shotcrete. In: 2006 NZSEE Conference paper